




Cell aggregation is associated with enzyme secretion strategies in marine polysaccharide-degrading bacteria

Journal Article

Author(s):

D'Souza, Glen Gerald ; Ebrahimi, Ali; Stubbusch, Astrid Katharina Maria ; Daniels, Michael; Keegstra, Johannes ; Stocker, Roman; Cordero, Otto; Ackermann, Martin

Publication date:

2023-05

Permanent link:

<https://doi.org/10.3929/ethz-b-000602761>

Rights / license:

[Creative Commons Attribution 4.0 International](#)

Originally published in:

The ISME Journal 17(5), <https://doi.org/10.1038/s41396-023-01385-1>

Funding acknowledgement:

169978 - A microscale analysis of the causes and consequences of the spatial arrangement of biological functions in microbial consortia (SNF)

ARTICLE OPEN



Cell aggregation is associated with enzyme secretion strategies in marine polysaccharide-degrading bacteria

Glen D'Souza^{1,2}✉, Ali Ebrahimi³, Astrid Stubbusch^{1,2}, Michael Daniels^{1,2}, Johannes Keegstra⁴, Roman Stocker⁴, Otto Cordero³ and Martin Ackermann^{1,2,5}

© The Author(s) 2023

Polysaccharide breakdown by bacteria requires the activity of enzymes that degrade polymers either intra- or extra-cellularly. The latter mechanism generates a localized pool of breakdown products that are accessible to the enzyme producers themselves as well as to other organisms. Marine bacterial taxa often show marked differences in the production and secretion of degradative enzymes that break down polysaccharides. These differences can have profound effects on the pool of diffusible breakdown products and hence on the ecological dynamics. However, the consequences of differences in enzymatic secretions on cellular growth dynamics and interactions are unclear. Here we study growth dynamics of single cells within populations of marine *Vibrionaceae* strains that grow on the abundant marine polymer alginate, using microfluidics coupled to quantitative single-cell analysis and mathematical modelling. We find that strains that have low extracellular secretions of alginate lyases aggregate more strongly than strains that secrete high levels of enzymes. One plausible reason for this observation is that low secretors require a higher cellular density to achieve maximal growth rates in comparison with high secretors. Our findings indicate that increased aggregation increases intercellular synergy amongst cells of low-secreting strains. By mathematically modelling the impact of the level of degradative enzyme secretion on the rate of diffusive oligomer loss, we find that enzymatic secretion capability modulates the propensity of cells within clonal populations to cooperate or compete with each other. Our experiments and models demonstrate that enzymatic secretion capabilities can be linked with the propensity of cell aggregation in marine bacteria that extracellularly catabolize polysaccharides.

The ISME Journal (2023) 17:703–711; <https://doi.org/10.1038/s41396-023-01385-1>

INTRODUCTION

Complex polysaccharides represent the largest pools of metabolizable resources that microbial populations encounter in their environment. The degradation of these polysaccharides by bacteria drives major biogeochemical processes such as the remineralization of particulate organic matter [1–3]. There are two general strategies of how bacteria degrade polysaccharides. A first strategy is degradation with periplasmic enzymes, so that only a small fraction of the hydrolysis products is lost to the extracellular environment [4–6]. This strategy has been referred to as “selfish” and is abundant in natural environments [2, 4–6].

Another common strategy by bacteria is to degrade polysaccharides using cell-surface-attached or released enzymes [2]. This generates a pool of hydrolysis products of low molecular weight, i.e. public goods that are freely diffusible [1–3]. Degradation products produced by one cell thus have the potential to influence the growth and metabolism of neighboring cells [1, 7–9] or diffuse away from the local microenvironment [10–12]. The rate at which degradation products diffuse and the local cell density can determine the potential benefits to the producer populations [13, 14]. A strategy by bacteria in nature to reduce diffusional losses

is to evolve mechanisms such as cell aggregation, thereby increasing local cell density and increasing the proportion of degradation products than can be taken up by the producer population [14–17]. This group behavior can allow cells to benefit from the degradative activities of other cells and enhance growth of the clonal population while growing on polysaccharides [13, 16].

Closely related strains can show marked differences in the repertoire of enzymes and the associated molecular mechanisms to utilize complex polysaccharides [5, 18]. For instance, marine *Vibrionaceae* strains differ in the secretion of extracellular alginate lyases that degrade alginate, a marine algae-derived polysaccharide composed of alternating units of guluronic acid and mannuronic acid [18, 19]. A prime example is of two *Vibrio splendidus* strains: 13B01 and 12B01. While 13B01 secretes high levels of alginate lyases, 12B01 secretes lower levels, a behavior that likely arises because the enzymes are bound to the cell membrane [18]. While it is known that the level of secretion of alginate lyases by *Vibrionaceae* strains influences population growth dynamics in well-mixed environments [18], it is generally unclear how differences in enzymatic secretion influence the behavior of individual cells. Studying these dynamics at the microscale will provide a better

¹Microbial Systems Ecology Group, Institute of Biogeochemistry and Pollutant Dynamics, Department of Environmental Systems Sciences, ETH Zurich, 8006 Zurich, Switzerland.

²Department of Environmental Microbiology, Eawag: Swiss Federal Institute of Aquatic Sciences, 8600 Dübendorf, Switzerland. ³Department of Civil and Environmental Engineering, MIT, Cambridge, MA 02139, USA. ⁴Institute of Environmental Engineering, Department of Civil, Environmental and Geomatic Engineering, ETH Zurich, 8093 Zurich, Switzerland. ⁵EPFL, School of Architecture, Civil and Environmental Engineering, Lausanne, Switzerland. ✉email: glengeralddsouza@gmail.com

Received: 22 April 2022 Revised: 6 February 2023 Accepted: 13 February 2023

Published online: 22 February 2023

understanding of intercellular interactions within bacterial aggregates, a growth behavior commonly observed when bacteria grow on polysaccharides [15, 16, 19, 20]. In this study, we sought to address these knowledge gaps by asking how the level of alginate lyase secretion influences aggregation and the growth dynamics of cells growing on polysaccharides.

We studied 12 marine *Vibrionaceae* isolates that have previously been shown to differ in the types and number of alginate lyases encoded in their genome [18]. They also differ in the total amount of these enzymes that are produced and secreted [18, 19]. These strains were previously isolated from marine habitats and span three distinct species: *Vibrio splendidus*, *Vibrio cyclitrophicus*, and *Vibrio* sp. F13 [18] (Supplementary Table 1). We first studied well-mixed batch cultures to determine whether population growth dynamics of the *Vibrionaceae* isolates are associated with the amount of alginate lyases that are produced and secreted. We then used microfluidics coupled to time-lapse microscopy [16] in order to quantify aggregation and single-cell growth dynamics of strains growing on alginate. Finally, we used mathematical modelling to analyse the influence of enzyme activity on polysaccharide breakdown and cellular interactions. Together, these experiments and models show that differences in the secretion of alginate lyases between strains are associated with differences in the aggregative behaviors and density-dependence of growth rates of bacterial populations.

RESULTS AND DISCUSSION

Strains belonging to the same species display distinct growth dynamics on the marine polysaccharide alginate

We first quantified the growth dynamics of the 12 *Vibrionaceae* strains (Supplementary Table 1) on alginate in well-mixed batch cultures. Growth of populations was initiated at approximately the same inoculum density (10^5 colony forming units (c.f.u.) ml^{-1}). We tracked the growth dynamics by measuring the optical density at 600 nm and compared the maximum population size reached over the course of 36 h (Fig. 1 and S1). We found significant differences in the maximal optical density achieved by different strains within each species (Fig. 1 and S1). In *V. splendidus*, strains 12B01 and FF6 reached a lower maximum population size compared to strains 1S124 and 13B01 (Fig. 1 and S1A). In *V. cyclitrophicus*, strain ZF270 reached a lower maximum population size compared to strains 1F175, 1F111, and ZF28 (Fig. 1 and S1A). Similarly, in *V. sp. F13*, strain 9ZC77 reached a lower maximum population size than strains 9CS106, 9ZC13, and ZF57 (Fig. 1 and S1A). These findings suggest that some strains are limited in their growth abilities in well-mixed environments, perhaps as a consequence of differences in the amount and activity of enzymes they release (Supplementary Table 1).

Differences in enzyme secretion are associated with differences in the growth dynamics of alginate degraders

We hypothesized that reduced secretion of alginate lyases is responsible for limiting the growth of strains that achieve low optical densities in batch culture (Fig. 1). To test our prediction, we measured the level of secretions of alginate degrading enzymes by the different strains using a plate assay. In this assay, alginate reacts with iodine to produce a violet compound. The breakdown of alginate by secreted enzymes that diffuse away from the colony creates simpler oligomers or monomers that yield colorless halos when stained with iodine (Fig. S2A). Therefore, the level of enzyme secretion and activity can be quantified by measuring the size of the alginate-free halo generated by cell colonies as they grow on an alginate-containing plate (see Methods and Fig. S2A) [21]. Strains that do not produce halos but can grow on alginate likely possess enzymes that are bound to the membrane or cell-surface. While this assay provides a quantitative measure of the activities of secreted enzymes, it cannot be used to determine the amount

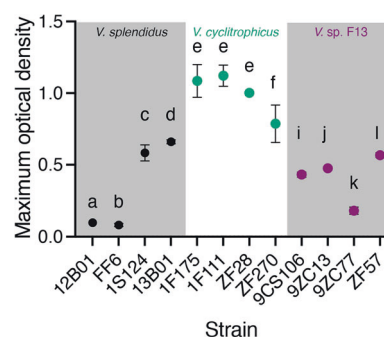


Fig. 1 *Vibrionaceae* strains differ in their growth dynamics on the marine polysaccharide alginate under well-mixed conditions.

Maximum optical density (measured at 600 nm) achieved by populations of strains belonging to *Vibrio splendidus*, *Vibrio cyclitrophicus*, and *Vibrio* sp. F13 during the course of a 36 h growth cycle on the same concentration (0.1% weight/volume) of the polysaccharide alginate. Points and error bars indicate the mean of measurements across populations within each ecotype ($n_{\text{populations}} = 3$) and the 95% confidence interval (CI), respectively. Different letters indicate statistically significant differences between strains within one species (One-way ANOVA and Dunnett's post-hoc test; *V. splendidus*: $p < 0.0001$, $F = 325.9$, $R^2 = 0.99$; *V. cyclitrophicus*: $p = 0.0099$, $F = 7.60$, $R^2 = 0.74$; *V. sp. F13*: $p < 0.0001$, $F = 245$, $R^2 = 0.98$). For growth curves of individual strains, see Fig. S1.

of enzymes secreted, since a lower quantity of highly active enzymes and a higher quantity of less-active enzymes could give the same clearing radius.

Enzyme secretion as measured by halo diameter varied among strains within each species. Among *V. splendidus* strains, 12B01 and FF6 had the lowest halo diameters (Fig. S2B), while among *V. cyclitrophicus* strains, ZF28 had a smaller halo diameter than the other strains (Fig. S2B). In contrast to the other *V. sp. F13* strains, 9ZC77 did not produce a detectable halo (Fig. S2B). This observation suggests that 9ZC77 either does not produce substantial enzymatic secretions or the alginate lyases are primarily membrane- or cell-surface bound. Comparison of the results from the plate assays (Fig. 2A, Fig. S2) and the batch cultures (Fig. 1) reveals that the level of secretion of alginate lyases by the different strains is significantly correlated with the maximum population size they achieved when growing on alginate under well-mixed conditions (Fig. 2A). This correlation supports our hypothesis that growth in batch culture is limited by the ability to produce secreted alginate lyases.

To further test our prediction that alginate lyase production capability constrains growth, we determined whether externally supplementing alginate lyases could alleviate the growth limitation of the strains that are low enzyme secretors. We grew the 12 strains individually as batch cultures in alginate medium that was supplemented with a commercial mixture of alginate lyases and measured their growth dynamics. The results show that alginate lyase supplementation did not alter the maximum population size reached by the low secreting strains (Fig. S3A). Commercial alginate lyases likely produce a mixture of oligomers and not just monomers. Therefore, cells of lower-growing alginate degraders could still be limited by the availability of monomeric hydrolysis products. We then calculated the time to reach exponential growth phase of each ecotype when growing in the presence of external alginate lyases and compared this with the time taken in the absence of this external supplementation. We found that the strains with a low level of enzyme secretion and activity, such as 12B01, FF6 and 9ZC77, showed the largest reduction in the time required to reach exponential phase upon supplementation with external alginate lyases (Fig. 2B and S3B, C). However, strains 12B01 and FF6 still have very low optical densities in these culture conditions, even in the presence of

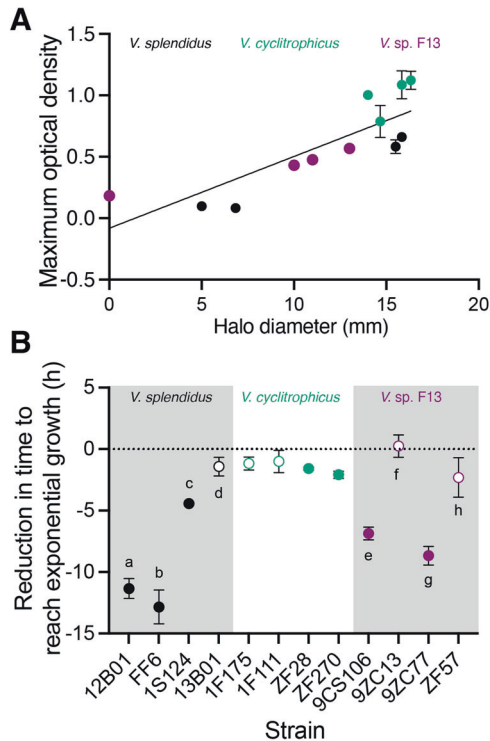


Fig. 2 Enzyme secretion capabilities govern growth dynamics of alginate degraders. **A** Correlation between maximum optical density in batch culture (Fig. 1) and halo diameters in the plate assays across the 12 strains. The line indicates the fit of a linear regression (slope = 0.05, $R^2 = 0.67$, $P < 0.0001$; Spearman's correlation: $r = 0.90$, $P = 0.0002$). **B** Supplementation with external alginate reduces the time to reach exponential growth phase of strains that secrete low levels of alginate lyase to a greater extent compared to high secretors of alginate lyase. Circles represent the mean of the populations of each ecotype ($n_{\text{populations}} = 3$) and error bars indicate 95% confidence intervals. Letters indicate statistically significant differences between strains within each species (One-way ANOVA with Dunnett's posthoc test; *V. splendidus*: $F = 114.0$, $p < 0.0001$, $R^2 = 0.97$; *V. cyclitrophicus*: $F = 2.36$, $p = 0.14$, $R^2 = 0.46$; *V. sp. F13*: $F = 47.27$, $p < 0.0001$, $R^2 = 0.94$). Open circles indicate non-significant differences from 0, indicating no reduction in the time to reach exponential phase; filled circles indicate significant differences from 0 (One sample *t*-test; 12B01: $t = 24.4$, $df = 2$, $p = 0.001$; FF6: $t = 16.1$, $df = 2$, $p = 0.003$; 1S124: $t = 53$, $df = 2$, $p = 0.004$; 13B01: $t = 3.2$, $df = 2$, $p = 0.08$; 1F175: $t = 3.8$, $df = 2$, $p = 0.06$; 1F111: $t = 1.9$, $df = 2$, $p = 0.19$; ZF28: $t = 19$, $df = 2$, $p = 0.002$; ZF270: $t = 3.8$, $df = 2$, $p = 0.006$; 9CS106: $t = 23$, $df = 2$, $p = 0.0019$; 9ZC13: $t = 0.4$, $df = 2$, $p = 0.67$; 9ZC77: $t = 19.6$, $df = 2$, $p = 0.002$; ZF57: $t = 2.4$, $df = 2$, $p = 0.13$). See Fig. S3 for growth dynamics of each ecotype on alginate as well as correlations between enzyme secretion and growth kinetics.

externally added enzymes, suggesting factors other than enzyme production limit the growth of these strains.

Strains with relatively higher enzyme secretions such as 9CS106, ZF57 and 9ZC13 showed varying levels of benefits from enzyme supplementation. It is known that such differences can emerge due to variations in enzyme catalytic properties, transport efficiencies and physiological properties of the different strains [5, 22]. In contrast to the effect of enzyme supplementation for *V. splendidus* and *V. sp. F13*, the effect of enzyme supplementation was more limited in *V. cyclitrophicus* (Fig. 2A), the species in which differences in enzyme activity were most limited (Figs. S2B, S3A, D). Taken together, our results suggest that strains that secrete low levels of alginate lyases benefit the most from external alginate lyase supplementation, indicating that the growth rate of these strains is limited by the ability to produce alginate lyases.

Strains with low levels of enzyme secretion display higher levels of aggregation in environments that favor spatial structure

Cell aggregation can reduce the growth limitations observed on polysaccharides in absence of supplementation and based on native enzymatic ability of strains [16]. Specifically, we expect that by reducing dispersal and forming aggregates, cells could reduce the diffusional loss of alginate lyases or breakdown products and thereby could alleviate growth limitation of strains with low secretion levels (we use the term "aggregate" here without implying that cells are actively moving towards each other; cell aggregates can also be formed if cells do not disperse after cell division, as observed previously [16]). We tested this prediction on a subset of the original 12 *Vibrionaceae* strains. From each species, we selected a representative ecotype producing high levels of alginate lyase (*V. splendidus*: 13B01; *V. cyclitrophicus*: 1F111; and *V. sp. F13*: 9ZC13) and one producing low levels of alginate lyase (*V. splendidus*: 12B01; *V. cyclitrophicus*: ZF270; and *V. sp. F13*: 9ZC77). To test if strains aggregate when growing on the polysaccharide alginate, we grew cells of the different strains within microfluidic growth chambers. Within these chambers cells receive a constant supply of alginate and divide, either forming aggregates by growing as monolayers or dispersing after division. This approach enabled the quantification of growth and movement using time-lapse microscopy coupled to automated image analysis.

We found that aggregative behaviors were common in all the strains across the three species tested (Fig. 3A–F). By following the growth dynamics of individual cells using cell segmentation and tracking, we were able to map lineages of all cells present in each growth chamber based on division events. This analysis revealed that cells emerging from the same founder cell tended to remain close to each other (Fig. 3A–F, Supplementary Video 1–6). However, for all three species, the low-secreting strains, (Fig. 3G–I), displayed a higher degree of aggregation compared to the corresponding high-secreting strains, 13B01 (Fig. 3G), 1F111 (Fig. 3H), and 9ZC13 (Fig. 3I). The maximum number of cells within aggregates in a chamber was on average 5.54, 3.21, and 1.89 times higher for the low-secreting strains of *V. splendidus*, *V. cyclitrophicus*, and *V. sp. F13*, respectively, compared to the corresponding high-secreting strains (Fig. S4). These findings indicate that cells of low-secreting strains, at least in the context of the three species-pairs tested, form larger aggregates while growing on alginate.

Density dependence is stronger in strains with low alginate lyase secretions

Given that low secretion by strains is associated with greater aggregation, we then quantified if the differential aggregation behaviors of strains influence growth abilities of individual cells on the polysaccharide alginate. For this, we measured the growth rate of individual cells within microfluidic chambers using automated image analysis (Fig. S5A–C). We then analyzed the relationship between the median growth rate of all the cells present in a chamber during a given time interval and the total number of cells that were present in the chamber during that interval. For cells of all six strains across three species, the median growth rate increases with the increase in the number of resident cells in a chamber up to a point, and then decreases as the number of cells increases further (Fig. 4). However, the number of cells required to achieve the maximal growth rate differed between the strains. For two of the three species tested, the maximal growth rate of the low-secreting ecotype occurred at a significantly higher cell density than that of the high-secreting ecotype (Fig. 4A, B, E, F). The comparison for *V. cyclitrophicus* did not follow this trend, with no significant difference between the two *V. cyclitrophicus* strains in the cell density associated with the maximal growth rate (Fig. 4C, D), likely because the two strains are much more similar in their level of secretion in comparison with the other species (Fig. 2A). The increased cell density due to aggregation within the

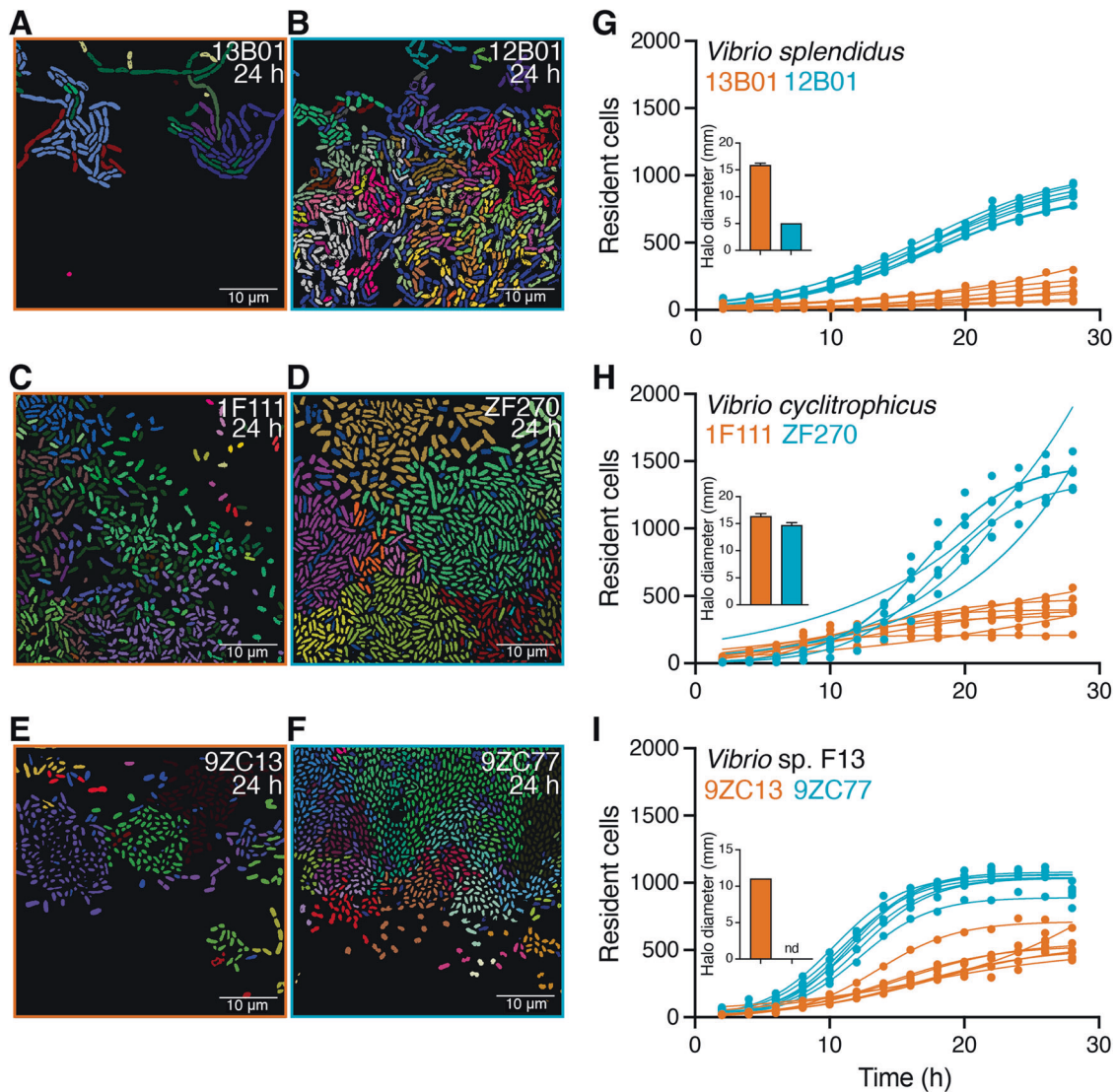


Fig. 3 Low enzymatic production is associated with stronger aggregation. Representative images of microfluidic growth chambers containing cells of (A) *Vibrio splendidus* 13B01, (B) *Vibrio splendidus* 12B01, (C) *Vibrio cyclitrophicus* 1F111, (D) *Vibrio cyclitrophicus* ZF270, (E) *Vibrio* sp. F13 9ZC13, and (F) *Vibrio* sp. F13 9ZC77. Cells that originate from the same founder cell are shown in the same color (based on cell tracking through divisions). The three high-secreting strains (13B01, 1F111 and 9ZC13) are shown with orange panel outlines and the three low alginate lyase secreting strains (12B01, ZF270 and 9ZC77) are shown with blue panel outlines. G–I The increase in the number of resident cells in growth chambers over time for strains of (G) *V. splendidus*, (H) *V. cyclitrophicus* and (I) *Vibrio* sp. F13. The levels of enzymatic secretions for the strains (from Fig. S2B) are shown in the inset of panels G–I. The number of cells in a chamber depends on both the rate at which cells divide and the fraction of cells that leaves the chamber. Circles indicate the number of cells present at a given time point in each chamber ($n_{\text{chambers}} = 7$), with a logistic growth regression line for each chamber: 13B01, $R^2 = 0.97\text{--}0.99$, max cells (mean \pm standard deviation) = 156.90 ± 83.21 , $k = 0.09\text{--}0.20 \text{ h}^{-1}$; 12B01, $R^2 = 0.99$ in all cases, max cells = 858.70 ± 67.78 , $k = 0.18\text{--}0.20 \text{ h}^{-1}$; 1F111, $R^2 = 0.89\text{--}0.99$, max cells = 410.40 ± 106.40 , $k = 0.10\text{--}0.53 \text{ h}^{-1}$; ZF270, $R^2 = 0.86\text{--}0.99$, max cells = 1318 ± 198.70 , $k = 0.10\text{--}0.30 \text{ h}^{-1}$; 9ZC13, $R^2 = 0.91\text{--}0.99$, max cells = 545.40 ± 50.69 , $k = 0.08\text{--}0.21 \text{ h}^{-1}$; 9ZC77, $R^2 = 0.98\text{--}0.99$, max cells = 1033 ± 72.12 , $k = 0.36\text{--}0.40 \text{ h}^{-1}$). See supplemental videos S1–S6 for timelapse image series of cells.

microfluidic chambers allows cells to overcome growth limitations that strains face in well-mixed environments (Fig. S6A). We find that high-secreting strains have similar or increased final growth rates compared to the low-secreting strains when growing in microfluidic chambers. This indicates that reduced group sizes of high-secreting strains (Fig. 3G–I) arise as a result of increased dispersal rather than reduced growth rates. Well-mixed environments, as in the batch-culture experiments, limit the growth rate of the two strains with the lowest levels of enzyme secretion, 12B01 and 9ZC77, relative to their high-secreting counterparts, 13B01 and 9ZC13, respectively (Fig. S6B). In contrast to growth in well-mixed environments, growing in spatially structured environments, such as within the microfluidic growth chambers, 12B01

and 9ZC77 are able to improve growth substantially relative to 13B01 and 9ZC13, respectively (Fig. S6B). The growth of 12B01 in microfluidic chambers is especially interesting since the growth of this strain was negligible in well-mixed environments (Fig. 1) even though it produced enzymes (Fig. S2B). These observations are indicative of other yet unknown biological factors that likely influence growth on polymers. In addition, 9ZC77 cells had no noticeable enzyme secretions (Fig. S2B) but displayed density dependent growth dynamics. This finding suggests that strains with cell-bound enzymes have a disadvantage in well-mixed environments but can benefit from surface-association. The growth rate of *V. cyclitrophicus* ecotype ZF270 relative to that of ecotype 1F111 is similar in both well-mixed and microfluidic

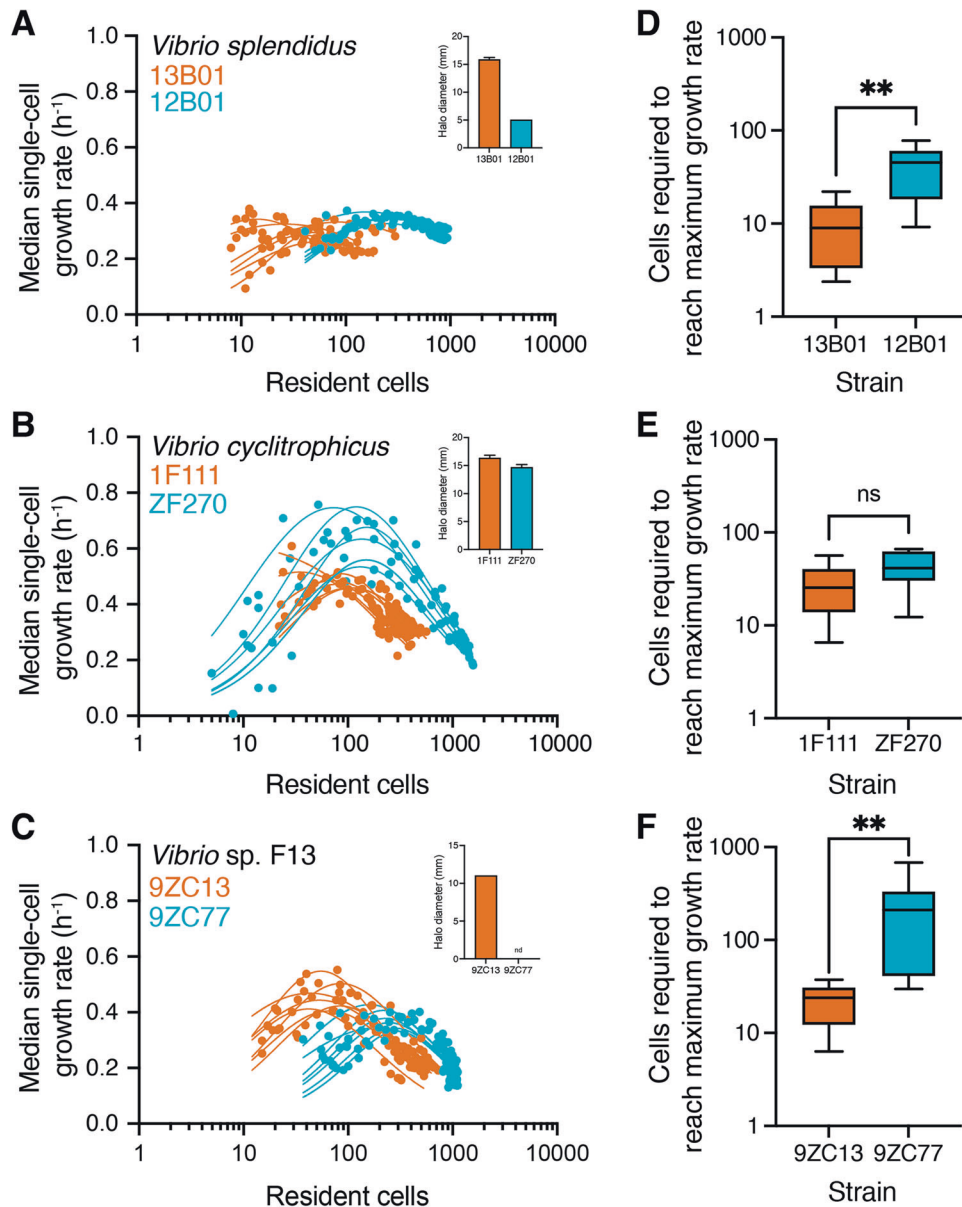


Fig. 4 Strains with low levels of enzyme secretion rely on an increased intercellular synergy during aggregative growth. **A–C** Median single-cell growth rate (h^{-1}) of **(A)** *Vibrio splendidus*, **(B)** *Vibrio cyclitrophicus* and **(D)** *Vibrio sp.* F13 cells as a function of the number of cells growing together in a microfluidic chamber. Cells were binned into 2-hour intervals based on their birth times over a 28 h experiment. This approach also yielded the number of cells present during growth in each time interval. The relationship between median growth rate of all cells present in a 2 h interval in a given chamber and the number of cells in the chamber was determined using a non-linear regression model for each chamber. The levels of enzymatic secretions for the strains (from Fig. S2B) are shown in the inset of panels. High-secretion strains are indicated in orange whereas relatively low-secretion strains are indicated in blue. Circles represent data for a single bin from one chamber, and lines indicate the trajectory of growth rates for each chamber ($n_{\text{chambers}} = 7$; 13B01, $R^2 = 0.52\text{--}0.76$; 12B01, $R^2 = 0.66\text{--}0.95$; 1F111, $R^2 = 0.88\text{--}0.91$; ZF270, $R^2 = 0.71\text{--}0.93$; 9ZC13, $R^2 = 0.73\text{--}0.95$; 9ZC77, $R^2 = 0.57\text{--}0.80$). **D–F** Number of cells required to reach half of the maximum growth rate for strains of **(D)** *V. splendidus*, **(E)** *V. cyclitrophicus*, and **(F)** *V. sp.* F13. The low-secreting *V. splendidus* ecotype 12B01 required a five-fold higher number of cells to achieve maximal growth rates compared to the high-secreting 13B01 cells (**D**; 13B01 median 8.99 cells and 12B01 median 45.25 cells). In the case of *V. cyclitrophicus*, both strains required a similar number of cells to reach maximal growth rates (**E**; 1F111 median 25.48 cells and ZF270 median 41.34 cells). For *V. sp.* F13, the low-secreting ecotype 9ZC77 required an eight-fold higher cell number to achieve maximal growth rates compared to the high-secreting ecotype 9ZC13 (**F**; 9ZC13 median 23.90 cells and 9ZC77 median 210.40 cells). Asterisks indicate statistically significant differences ($P < 0.001$) between strains (Mann–Whitney tests, $n_{\text{chambers}} = 7$; *V. splendidus*, $p = 0.008$, Hodges–Lehmann difference = 36.75; *V. cyclitrophicus* $p = 0.15$, Hodges–Lehmann difference = 19.85; *V. sp.* F13 $p = 0.003$, Hodges–Lehmann difference = 188.5). Box plots extend from the 25th to 75th percentiles and whiskers indicate the 10th and 90th percentiles of median growth rates.

growth environments (Fig. S6B). These findings indicate that surface association and aggregate formation allow strains, especially those that secrete very low levels of alginate lyases, to increase cell density and enables cells to benefit from each other's degradation activities, thereby allowing intercellular synergy

amongst cells within aggregates in spatially structured environments. The increased cell density and surface-association thus enables cells in spatially structured environments to overcome growth limitations that arise when growing on polysaccharides in well-mixed environments.

Once the growth rate has reached its maximum value, the growth rate then plateaus for *V. splendidus* strains or begins to decrease for *V. cyclitrophicus* and *V. sp. F13* strains with further increase in the cell numbers within the growth chambers (Fig. 4A, C, E). We measured the peak cell densities reached within the growth chambers (13B01: 250.30 ± 129 (mean cell number across replicate chambers \pm standard deviation), 12B01: 1439 ± 98.95 , 1F111: 255 ± 42.85 , ZF270: 418.60 ± 34.11 , 9ZC13: 228.80 ± 39.61 and 9ZC77: 358.5 ± 109.10) and found that the benefit of intercellular interactions is balanced (for *V. splendidus*) or outweighed (for *V. cyclitrophicus* and *V. sp. F13*) by the negative effects of competitive interactions between cells within aggregates.

Since maximum growth rates are dependent on cell densities, we probed if an increased initial inoculum density would allow low-secreting strains to increase growth rates in well-mixed batch culture environments. In line with our findings in microfluidic chambers, low-secreting strains 12B01 and 9ZC77 benefit from a higher inoculum density (Fig. S7A–C). An increased inoculum density reduces the growth rate of high-secreting strains in well-mixed environments (Fig. S7A–C). These findings lend further credence to our idea that high cell densities due to aggregate formation can benefit low enzyme secreting strains.

A mathematical model offers a mechanistic explanation for the role of cell density and enzyme secretion on polymer degradation and growth rates

To obtain a mechanistic understanding of the roles of cell density and enzyme secretion rate on growth rates of strains, we developed an individual-based model of the growth rate of cells on polysaccharides taking into account cell density, enzymatic breakdown and loss of breakdown products. Our goal was to describe a system composed of spatially structured populations in nature similar to cells growing as a monolayer in microfluidic growth chambers. We modeled a 2D system (Supplementary Information and Table S2) where cells occupy sites on a 50×50 grid (Fig. 5A). We assumed diffusion as the mode of transport within the 2D chamber for polymeric substrates, secreted enzymes, and breakdown products. The loss of breakdown products (oligomers) and enzymes from the opening of the chamber by flow is simulated by assuming constant zero concentrations as the boundary condition. Individual cells are initially uniformly distributed on the 2D lattice, where they secrete enzymes that breakdown polysaccharides, consume oligomers, and grow in response to local oligomer concentrations. Monod-type kinetics were used to model substrate uptake and cell growth (see methods for details). The rate of enzyme secretion, S_E , was assumed to follow first-order kinetics as a function of cell biomass, $S_E = K_{enz}B$, as previously observed experimentally, where K_{enz} is the enzymatic activity and an intrinsic cellular property and B is the individual cell biomass.

We asked whether our model predicts similar density-dependent growth dynamics to those observed in the experimental observations. We simulated bacterial growth in the 2D chambers and calculated the mean growth rates over a wide range of initial cell densities and enzymatic activities. Consistent with our experimental observations, the model predicted that the growth rate of cells with lower enzymatic activity is higher at an increased cell density (Fig. 5B). In comparison, cells with a higher enzymatic activity through increased secretions have higher growth rates at low densities (Fig. 5B). To understand the biophysical mechanism underlying these effects, we examined the spatial profile of oligomer concentrations simulated by the model and found that lower enzymatic activity leads to the accumulation of oligomers and supports higher growth rates for cells regardless of their spatial arrangement. However, in higher enzymatic activity, oligomers arising as result of polysaccharide degradation are increasingly lost to diffusion without being available for bacterial cells to uptake (Fig. 5C). Our results indicate that the rate of oligomer loss to diffusion and uptake plays a dominant role in shaping the nature of

intercellular interactions in polysaccharide-degrading populations. We thus performed simulations where the diffusion coefficients of polymers and oligomers were systematically varied relative to diffusion in free water to yield low rates of diffusion such as in biofilm or cell aggregations and high rates of diffusion similar to boundary conditions in a quiescent region in contact with flow. The model suggests that a scenario with a diffusion coefficient that is an order of magnitude lower than that in bulk water results in the highest average growth rate for the bacterial population (Fig. 5DE). A higher diffusion rate that resembles flow, while increasing the polymer degradation rate (Fig. 5D), also enhances the loss of oligomers through diffusion, making them unavailable to bacterial cells and thus reducing the growth rate. A similar effect emerges at higher cell densities, where faster polymer degradation by cells at the opening of the growth chambers can result in loss of oligomers, thereby making them unavailable to other cells and leads to negative density dependent growth effects (Fig. 5C, E). In absence of experimental measurements, constant physiological properties for maximum growth rate, half-saturation constant and yield of converting oligomers to biomass were assumed for all bacterial cell types. Recent studies had shown variabilities in half-saturation constant across bacterial strains [5] and further studies are required to investigate the role of these physiological differences on bacterial collective behavior.

Our results indicate that enzymatic secretion capabilities can influence growth dynamics and intercellular interactions within bacterial populations growing on polysaccharides. Differences in enzyme secretion levels can arise as a result of strains harboring functionally distinct alginate lyases or as a result of distinct localization of alginate lyases [18, 22–24]. For instance, as previously explained *V. splendidus* 12B01 has alginate lyases that are largely intra-cellular or membrane-bound whereas alginate lyases of *V. splendidus* 13B01 are largely secreted into the extracellular environment [18, 25]. In addition, strains can harbor distinct classes of alginate lyases and the breakdown products generated by these enzymes can differ [26]. Our findings suggest that cells that are genetically predisposed to produce low levels of enzymes or have predominantly membrane-bound alginate lyases can overcome growth disadvantages that exist in well-mixed environments by aggregating. These collective behaviors allow cells to generate 5–10-fold higher local cell densities enabling growth at maximal rates. Differences in growth patterns between rumen-derived strains of *Bacteroides thetaiotaomicron* on the polysaccharide yeast α -mannan have also been shown to emerge as a consequence of variation in substrate uptake affinities [5]. Our finding that supplementation of alginate lyase, which should increase the pool of oligo- or monomeric hydrolysis products, did not increase maximum growth yields of the low alginate lyase secreting strains suggests that uptake capabilities of strains could also play a part in the observed growth constraints on polymers.

Polysaccharides like alginate or chitin exist predominantly as particulates in natural ecosystems [27] and offer surfaces that enable bacterial cells to form dense colonies. It is known that surface association can induce the expression of polysaccharide utilization genes in bacterial populations [28]. In addition, aggregation behaviors increase local cell densities and enable intercellular interactions that can allow individuals to benefit from each other's metabolic activities [16, 29]. Strains that have increased enzymatic secretions can breakdown polysaccharides by adopting dispersed growth modes, that can facilitate migration of cells to new polysaccharide particles in nature. Additionally, in communities where multiple strains coexist [7, 8, 20, 30], the degradative activity of high enzyme secretors can create public goods that can positively influence the growth of not only the low enzyme producers but also strains that lack the ability to degrade polysaccharides and rely on cross-feeding of monomers from the polymer degraders [18, 31, 32].

Dispersal and collective behaviors have been shown to evolve together in multiple organisms [33, 34]. Differences in mobility can

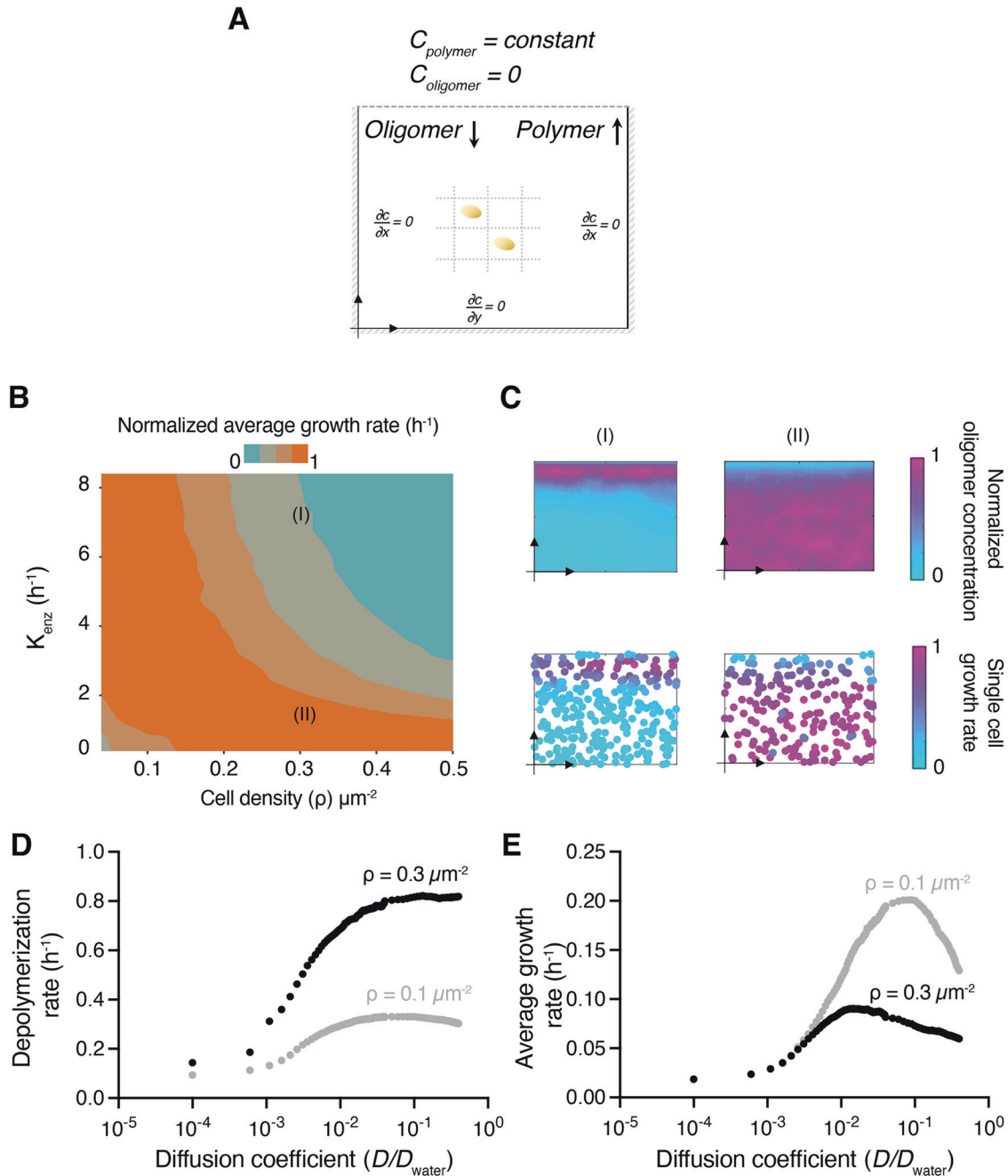


Fig. 5 A mathematical model illustrates the biophysical mechanisms underlying bacterial density-dependent growth on polysaccharides. **A** Schematic representation of the mathematical model that simulates microfluidic chambers as a 2D lattice with $50 \times 50 \mu\text{m}$ grid. Individual cells occupy single grid cells where they act as sink terms for the oligomer diffusion–reaction model. A Dirichlet boundary condition is used at the chamber periphery to simulate the effect of flow, which allows for constant concentrations of polysaccharide (0.1 mg/L) and oligomer (0 mg/L) at the boundary. Cells are uniformly distributed in the chamber. **B** Average growth rates of individual cells 20 h after the start of the simulations as a function of enzymatic activity, K_{enz} , and cell density, ρ . The growth rate was normalized to the maximum values obtained across the full set of conditions. **C** Oligomer profiles and single-cell growth rates for simulated chambers after 20 h. Two scenarios are shown, taken from simulations in Fig. 5B (I, $\rho = 0.3 \mu\text{m}^{-2}$ and $K_{\text{enz}} = 0.7 \text{ hr}^{-1}$; II, $\rho = 0.3 \mu\text{m}^{-2}$ and $K_{\text{enz}} = 0.1 \text{ h}^{-1}$). The values of growth rates and oligomer concentrations are normalized to the maximum values observed in the simulations to allow comparison. **D** Depolymerization and **E** growth rates of polysaccharides as a function of the diffusion coefficient of oligomers, polysaccharide, and enzymes. The diffusion coefficient was normalized by the diffusion coefficient in free water. Simulation parameters are described in detail in Table S2.

dramatically influence the likelihood of individuals in a population engaging in cooperation [33]. When the cost of aggregation behaviors is high, cooperation between individuals of a population is favored when individuals disperse less [34]. Less costly behaviors are relatively less sensitive to dispersal of individuals [34]. While aggregation behaviors do provide a benefit to

individuals that require high densities, increased dispersal can allow individuals that produce higher levels of public goods to avoid invasion by consumer cells which do not engage in public good production [35].

The cellular processes that link aggregation, motility and polymer metabolism in marine bacterial populations are yet unclear. The

formation of bacterial aggregates and production of polysaccharide-degrading enzymes both require substantial cellular resources and thus likely impose substantial metabolic costs on cells [10, 36]. This will result in cells facing trade-offs between allocating resources to enzyme production versus aggregation [14], both of which enable cells to grow on polymers. A potential consequence is that marine polysaccharide degraders are constrained by trade-offs such that they forego enzymatic capabilities in favor of aggregation or alternately acquire genes encoding enzymes that can either be produced in large amounts and also be secreted instead of aggregate formation capabilities. Aggregation of bacterial cells is known to be coordinated through quorum sensing [37, 38]. However, the molecular mechanisms that regulate collective behaviors in response to the nutrient composition in the natural environment are yet unclear. Our work is a first step in this direction and provides a direct link between the dynamics of enzyme secretion, growth physiology and collective behaviors of polysaccharide degrading bacterial populations.

MATERIALS AND METHODS

Bacterial strains, media, and batch culture growth assays

Experiments were performed using previously isolated *Vibrio splendidus* strains 13B01, 12B01, FF6 and 1S124; *Vibrio cyclitrophicus* strains 1F175, 1F111, ZF270 and ZF28; and *Vibrio* sp. F13 strains 9CS106, 9ZC13, 9ZC77 and ZF57 (Supplementary Table S1). These strains are deposited in the Culture Collection of Switzerland and freely available through them (See Table S1 for accession numbers). The isolation conditions and the genes encoding alginate lyases in these strains have been described previously [18]. Prior to experiments, strains were cultured in Marine Broth (MB medium, DIFCO) and grown for 18 h at 25 °C. Cells from these cultures were then used for batch culture growth kinetic assays in Tibbles–Rawling Minimal Medium [18, 39] (TR medium) containing 0.1% (weight/volume) alginate (Sigma Aldrich). Sterile alginate solution was prepared using nanopure water and filter sterilized using 0.40 µm surfactant-free cellulose acetate filters (Corning). For growth assays with enzyme supplementation, 0.05 units ml⁻¹ of alginate lyase (Sigma) was added to TR medium containing 0.1% alginate. Batch growth kinetic assays were performed in 96-well plates and growth was measured using a micro-well plate reader (Biotek). For this, 1 ml of cell suspension from a culture growing in MB medium was centrifuged (13,000 rpm for 2 min) in a 2 ml microfuge tube. The supernatant was discarded and the cell pellet was washed twice with TR medium without any carbon source. The cell pellet was resuspended in 500 µl of TR medium without carbon source and the optical density measured and adjusted to 0.1 OD. For the experiments, 5 µl of this OD-adjusted cell suspension was used to seed wells containing 195 µl TR minimal medium with the carbon source. Cells were allowed to grow for 40 h at 25 °C and OD measurements taken every 30 minutes. Each experiment was replicated 3–6 times.

Enzyme secretion assay

An agarose plate assay [21] was used to test the ability of strains to secrete alginate lyases. Prior to experiments, cultures were grown for 18 h in MB medium and 1 ml of cell suspension was centrifuged (13,000 rpm for 2 min) in a 2 ml microfuge tube. The supernatant was discarded and the cell pellet was washed twice with TR medium without any carbon source and then centrifuged. The cell pellet was suspended in 1 ml of TR medium without carbon source and the optical density measured and adjusted to 0.1 OD. For the assays, 50 µl of this culture was spotted on plates that were made using TR medium containing 0.1% (w/v) alginate and 1% agarose (Applichem). Colonies were allowed to grow for 30 h at 25 °C and then the plates were flooded with 2% Gram's iodine. Excess iodine was discarded and the plate imaged using a 12MP iPhone camera. If cells secreted alginate lyases, then a distinct clearance zone was formed, the diameter of which was measured using a ruler.

Microfluidics and time-lapse microscopy

The setup of microfluidics experiments has been described in detail previously [16, 29]. Cell growth and behavior was imaged within chambers measuring 60–120 × 60 × 0.56 µm (length × width × height). In these chambers, cells could adhere to the glass surface and experienced TR medium with 0.1% alginate that diffused into the lateral flow channels (0.1 ml h⁻¹).

Microscopy imaging was performed using an IX83 inverted microscope system with automated stage controller (Marzhauser Wetzlar), shutter, and laser-based autofocus system (Olympus ZDC 2). Chambers were imaged in parallel on the same PDMS chip, capturing phase-contrast images of each position every 8–10 min. Images were acquired using an UPLFLN 100x oil immersion objective (Olympus) and an ORCA-flash 4.0 v2 or v4 sCMOS cameras (Hamamatsu, Japan). For image acquisition, the CellSens 1.18 and higher software package (Olympus) were used. The microscopy units and PDMS chip were maintained at 25 °C using a cellVivo microscope incubation system (Pecon GmbH).

Image analysis

Cell segmentation and tracking was performed in ilastik (v1.2 and newer) [40]. The phase-contrast images were aligned using SuperSegger [41]. Images were cropped at the boundaries of each microfluidic chamber. Growth properties (cell area over time) and spatial locations (*x* and *y* coordinates) were directly derived using the ilastik Tracking plugin and using a custom algorithm (available in repository).

Datasets and statistical analysis

Growth curves were analyzed in Python (v3.8) using the AMiGA software [42] and GraphPad Prism v9 (GraphPad Software). The microscopy dataset set consists of seven chambers for each strain. These are grouped into two biological replicates wherein each biological replicate is fed by medium through one unique channel in a microfluidic chip, with three chambers fed by one channel and four chambers by another. Cells with negative growth rates (13B01 = 20%, 12B01 = 33%, 1F111 = 36%, ZF270 = 24%, 9ZC13 = 26%, 9ZC77 = 27%) were excluded from the analysis after visual curation, and represent artefacts, mistakes in linking during the segmentation process or non-growing deformed cells. In total, 2524 cells were analyzed for 13B01, 11547 cells for 12B01, 3227 cells for 1F111, 24444 cells for ZF270, 8910 cells for 9ZC13, and 24335 cells for 9ZC77. Each chamber was treated as an independent replicate. Each figure depicts medians of the seven chambers for each strain. Detailed equations for non-linear regression models for growth rate as a function of cell density are provided in Supplementary Methods. Comparisons were considered statistically significant when *p* > 0.05. FDR corrections were applied when multiple *t*-tests were performed for the same dataset. Measures of effect size are represented by the *R*² or *eta*² value. All statistical analyses were performed in either GraphPad Prism v 9.0 (GraphPad Software) or Rstudio v1.1.463 (Rstudio inc). All data analysis scripts are deposited along with the raw data.

DATA AVAILABILITY

All curated image analysis datasets and source data for figures are available on Zenodo (<https://doi.org/10.5281/zenodo.7032036>). Supplementary videos are available on figshare (<https://doi.org/10.6084/m9.figshare.20537685>).

REFERENCES

- Grondin JM, Tamura K, Déjean G, Abbott DW, Brumer H. Polysaccharide utilization Loci: Fueling microbial communities. *J Bacteriol.* 2017;199:e00860–16.
- Arnosti C, Wietz M, Brinkhoff T, Hehemann J-H, Probandt D, Zeugner L, et al. The biogeochemistry of marine polysaccharides: Sources, inventories, and bacterial drivers of the carbohydrate cycle. *Ann Rev Mar Sci.* 2021;13:81–108.
- Arnosti C. Microbial extracellular enzymes and the marine carbon cycle. *Annu Rev Mar Sci.* 2011;3:401–25.
- Reintjes G, Arnosti C, Fuchs B, Amann R. Selfish, sharing and scavenging bacteria in the Atlantic Ocean: A biogeographical study of bacterial substrate utilisation. *ISME J.* 2019;13:1119–32.
- Klassen L, Reintjes G, Tingley JP, Jones DR, Hehemann J-H, Smith AD, et al. Quantifying fluorescent glycan uptake to elucidate strain-level variability in foraging behaviors of rumen bacteria. *Microbiome.* 2021;9:23.
- Cuskin F, Lowe EC, Temple MJ, Zhu Y, Cameron EA, Pudlo NA, et al. Human gut *Bacteroidetes* can utilize yeast mannan through a selfish mechanism. *Nature.* 2015;517:165–9.
- Enke TN, Leventhal GE, Metzger M, Saavedra JT, Cordero OX. Microscale ecology regulates particulate organic matter turnover in model marine microbial communities. *Nat Comm.* 2018;9:2743.
- Cordero OX, Datta MS. Microbial interactions and community assembly at microscale. *Curr Opin Microbiol.* 2016;31:227–34.
- Cordero OX, Stocker RA. *particularly* useful system to study the ecology of microbes: Crystal ball. *Environ Microbiol Rep.* 2017;9:16–17.

10. Drescher K, Nadell CD, Stone HA, Wingreen NS, Bassler BL. Solutions to the public goods dilemma in bacterial biofilms. *Curr Biol* 2014;24:50–55.
11. Stewart PS, Franklin MJ. Physiological heterogeneity in biofilms. *Nat Rev Microbiol*. 2008;6:199–210.
12. Leventhal Gabriel E, Ackermann M, Schiessl Konstanze T. Why microbes secrete molecules to modify their environment: the case of iron-chelating siderophores. *J R Soc Interface*. 2019;16:20180674.
13. Driscoll WW, Pepper JW. Theory for the evolution of diffusible external goods. *Evolution*. 2010;64:2682–7.
14. Allison SD. Cheaters, diffusion and nutrients constrain decomposition by microbial enzymes in spatially structured environments. *Ecol Lett*. 2005;8:626–35.
15. Koschwanez JH, Foster KR, Murray AW. Improved use of a public good selects for the evolution of undifferentiated multicellularity. *eLife*. 2013;2:e00367.
16. D'Souza GG, Povolito VR, Keegstra JM, Stocker R, Ackermann M. Nutrient complexity triggers transitions between solitary and colonial growth in bacterial populations. *ISME J*. 2021;15:2614–26.
17. Tong K, Bozdogan GO, Ratcliff WC. Selective drivers of simple multicellularity. *Curr Opin Microbiol*. 2022;67:102141.
18. Hehemann J-H, Arevalo P, Datta MS, Yu X, Corzett CH, Henschel A, et al. Adaptive radiation by waves of gene transfer leads to fine-scale resource partitioning in marine microbes. *Nat Comm*. 2016;7:12860.
19. Ebrahimi A, Schwartzman J, Cordero OX. Multicellular behaviour enables cooperation in microbial cell aggregates. *Philos Trans R Soc Lond Ser B*. 2019;374:20190077.
20. Ebrahimi A, Schwartzman J, Cordero OX. Cooperation and spatial self-organization determine rate and efficiency of particulate organic matter degradation in marine bacteria. *Proc Natl Acad Sci USA*. 2019;116:23309–16.
21. Sawant SS, Salunke BK, Kim BS. A rapid, sensitive, simple plate assay for detection of microbial alginate lyase activity. *Enzym Micro Technol*. 2015;77:8–13.
22. Badur AH, Jagtap SS, Yalamanchili G, Lee J-K, Zhao H, Rao CV. Alginate lyases from alginate-degrading *Vibrio splendidus* 12B01 are endolytic. *Appl Environ Microbiol*. 2015;81:1865–73.
23. Ertesvåg H. Alginate-modifying enzymes: biological roles and biotechnological uses. *Front Microbiol*. 2015;6:523.
24. Inoue A, Takadono K, Nishiyama R, Tajima K, Kobayashi T, Ojima T. Characterization of an alginate lyase, FIALyA, from *Flavobacterium* sp. strain UMI-01 and its expression in *Escherichia coli*. *Mar Drugs*. 2014;12:4693–712.
25. Wargacki AJ, Leonard E, Win MN, Regitsky DD, Santos CNS, Kim PB, et al. An engineered microbial platform for direct biofuel production from brown macroalgae. *Science*. 2012;335:308.
26. Badur AH, Plutz MJ, Yalamanchili G, Jagtap SS, Schweder T, Unfried F, et al. Exploiting fine-scale genetic and physiological variation of closely related microbes to reveal unknown enzyme functions. *J Biol Chem*. 2017;292:13056–67.
27. Mühlenbruch M, Grossart H-P, Eigemann F, Voss M. Mini-review: Phytoplankton-derived polysaccharides in the marine environment and their interactions with heterotrophic bacteria. *Environ Microbiol*. 2018;20:2671–85.
28. Baty AM 3rd, Eastburn CC, Diwu Z, Techkarnjanaruk S, Goodman AE, Geesey GG. Differentiation of chitinase-active and non-chitinase-active subpopulations of a marine bacterium during chitin degradation. *Appl Environ Microbiol*. 2000;66:3566–73.
29. Dal Co A, van Vliet S, Kiviet DJ, Schlegel S, Ackermann M. Short-range interactions govern cellular dynamics in microbial multi-genotype systems. *Nat Ecol Evol*. 2020;4:366–275.
30. Enke TN, Datta MS, Schwartzman J, Cermak N, Schmitz D, Barrere J, et al. Modular assembly of polysaccharide-degrading marine microbial communities. *Curr Biol*. 2019;29:1528–e6.
31. Pontrelli S, Szabo R, Pollak S, Schwartzman J, Ledezma-Tejeida D, Cordero OX, et al. Metabolic cross-feeding structures the assembly of polysaccharide degrading communities. *Sci Adv*. 2022;8:eabk3076.
32. Amarnath K, Narla AV, Pontrelli S, Dong J, Caglar T, Taylor BR, et al. Stress-induced cross-feeding of internal metabolites provides a dynamic mechanism of microbial cooperation. *bioRxiv*. 2021; 2021.06.24.449802. <https://doi.org/10.1101/2021.06.24.449802>.
33. Smaldino PE, Schank JC. Movement patterns, social dynamics, and the evolution of cooperation. *Theor Popul Biol*. 2012;82:48–58.
34. Purcell J, Brelsford A, Avilés L. Co-evolution between sociality and dispersal: The role of synergistic cooperative benefits. *J Theor Biol*. 2012;312:44–54.
35. Taylor TB, Rodrigues AMM, Gardner A, Buckling A. The social evolution of dispersal with public goods cooperation. *J Evol Biol*. 2013;26:2644–53.
36. Takemura AF, Corzett CH, Hussain F, Arevalo P, Datta M, Yu X, et al. Natural resource landscapes of a marine bacterium reveal distinct fitness-determining genes across the genome. *Environ Microbiol*. 2017;19:2422–33.
37. Singh PK, Bartalomej S, Hartmann R, Jeckel H, Vidakovic L, Nadell CD, et al. *Vibrio cholerae* combines individual and collective sensing to trigger biofilm dispersal. *Curr Biol*. 2017;27:3359–e7.
38. van Gestel J, Barea T, Tenenbaum B, Dal Co A, Guler P, Aframian N, et al. Short-range quorum sensing controls horizontal gene transfer at micron scale in bacterial communities. *Nat Commun*. 2021;12:2324.
39. Tibbles BJ, Rawlings DE. Characterization of nitrogen-fixing bacteria from a temperate saltmarsh lagoon, including isolates that produce ethane from acetylene. *Micro Ecol*. 1994;27:65–80.
40. Sommer C, Straehle C, Kothe U, Hamprecht FA. Ilastik: Interactive learning and segmentation toolkit. *2011 IEEE International Symposium on Biomedical Imaging: From Nano to Macro*. 2011. IEEE, Chicago, IL, USA, pp 230–3.
41. Stylianidou S, Brennan C, Nissen SB, Kuwada NJ, Wiggins PA. *SuperSegger*: Robust image segmentation, analysis and lineage tracking of bacterial cells: Robust segmentation and analysis of bacteria. *Mol Microbiol*. 2016;102:690–700.
42. Midani FS, Collins J, Britton RA. AMiGA: Software for automated Analysis of Microbial Growth Assays. *mSystems*. 2021;4:e00508–21.

ACKNOWLEDGEMENTS

We thank Daan Kiviet and Susan Schlegel for designing the microfluidic growth chambers, and past and present members of the Microbial Systems Ecology group for feedback. This research was funded by an ETH fellowship and a Marie Curie Actions for People COFUND program fellowship (FEL-37-16-1) to GD; a Career Seed Grant from ETH Zurich to GD; the Simons Foundation Collaboration on Principles of Microbial Ecosystems (PriME #542389 and #542395) to MA, OC, and RS; a grant from the Swiss National Science Foundation (31003A_169978) to MA; and by ETH Zurich and EAWAG.

AUTHOR CONTRIBUTIONS

GD conceived the research along with MA, AE, and OC. AE developed the mathematical model and simulations along with OC. GD designed and performed all experiments. AS developed the algorithm to compute growth rates from the cell segmentation pipeline. GD analyzed the data with inputs from AE, JK, OC, RS, and MA. MD developed the alginate lyase detection assay based on previous literature. GD and AE wrote the manuscript with inputs from JK, AS, MD, RS, OC, and MA.

FUNDING

Open access funding provided by Swiss Federal Institute of Technology Zurich.

COMPETING INTERESTS

The authors declare no competing interests.

ADDITIONAL INFORMATION

Supplementary information The online version contains supplementary material available at <https://doi.org/10.1038/s41396-023-01385-1>.

Correspondence and requests for materials should be addressed to Glen D'Souza.

Reprints and permission information is available at <http://www.nature.com/reprints>

Publisher's note Springer Nature remains neutral with regard to jurisdictional claims in published maps and institutional affiliations.



Open Access This article is licensed under a Creative Commons

Attribution 4.0 International License, which permits use, sharing, adaptation, distribution and reproduction in any medium or format, as long as you give appropriate credit to the original author(s) and the source, provide a link to the Creative Commons license, and indicate if changes were made. The images or other third party material in this article are included in the article's Creative Commons license, unless indicated otherwise in a credit line to the material. If material is not included in the article's Creative Commons license and your intended use is not permitted by statutory regulation or exceeds the permitted use, you will need to obtain permission directly from the copyright holder. To view a copy of this license, visit <http://creativecommons.org/licenses/by/4.0/>.

© The Author(s) 2023